Biochemical and Biophysical Research Communications 378 (2009) 133–138

Contents lists available at ScienceDirect

Biochemical and Biophysical Research Communications

journal homepage: www.elsevier.com/locate/ybbrc

Reanalysis of structure/function correlations in the region of transmembrane segments 4 and 5 of the rabbit sodium/glucose cotransporter

Tiemin Liu, Pam Speight, Mel Silverman *

Department of Medicine, University of Toronto, Medical Sciences Building, Room 7336, 1 King's College Circle, Toronto, Ontario, Canada M5S 1A8

ARTICLE INFO

Article history:
Received 2 November 2008
Available online 20 November 2008

Keywords:
Glucose–galactose malabsorption
Methanethiosulfonate reagents
Secondary structure

ABSTRACT

The predicted topology of the mammalian high-affinity sodium/glucose cotransporter (SGLT1), in the region surrounding transmembrane segments 4 and 5, disagrees with the recent published crystal structure of bacterial SGLT from *Vibrio parahaemolyticus* (vSGLT). To investigate this issue further, 38 residues from I143 to A180 in the N-terminal half of rabbit SGLT1 were each replaced with cysteine and then expressed in COS-7 cells or *Xenopus laevis* oocytes. The membrane orientations of the substituted cysteines were determined by treatment with the thiol-specific reagent N-Biotinoylaminoethyl methanethiosulfonate (biotin-MTSEA), combined with the membrane impermeant thiol-specific reagent sodium (2-sulfonatoethyl) methanethiosulfonate (MTSES). The present results combined with previous structure/function studies of SGLT1, suggest that transmembrane domain (TM) 4 of mammalian SGLT1 extends from residue 143–171 and support the topology observed in the crystal structure of vSGLT.

The high-affinity sodium/glucose cotransporter (SGLT1) [1] is an active secondary transporter that utilizes the sodium electrochemical gradient to transport sugar substrates uphill against a concentration gradient. SGLT1 belongs to the homologous family of Na^+/solute symporters (SLC5) and is expressed most abundantly at the mucosal surface of the small intestine [2,3]. It serves as the principal uptake pathway for glucose derived from dietary sources. Mutations that result in dysfunctional SGLT1 affect intestinal glucose/galactose absorption [1]. Recently, SGLT1 has been a target protein for diabetes treatment [4].

The transporter functions as a monomer with 14 transmembrane domains (Fig. 1) and exhibits a stoichometry of 2 Na^+ ions: 1 sugar molecule [5]. Investigation of the structure/function relationships of SGLT1 is crucial to understanding cotransporter mechanism [6–10].

The recently published crystal structure of *Vibrio parahaemolyticus* SGLT (vSGLT) contains a core structure formed by multiple transmembrane helices from both N-terminus (TMs 2–6) and C-terminus (TMs 7–11) [11]. Galactose and Na^+ are bound in the center of the core. Both SGLT1 and vSGLT belong to the solute sodium symporters family, have a sequence similarity of 60%, contain 14 transmembrane domains and share an alternating-access mechanism with tight coupling between sodium and solute transport [11]. This suggests that they may have similar structure and function. However, the validity of extrapolating the structure of vSGLT to mammalian SGLT1 is brought into question. Previous biochemical characterization of SGLT1 showed that TMs 10–13 in the C-terminal half of SGLT1 retained sufficient tertiary structure to transport sugar downhill in a stereospecific and selective manner [8]. On the other hand, studies from other groups suggest that the putative external loop joining TM 4–5 in the N-terminal half of SGLT1 is involved in the Na^+ interaction [6,12–14] and TM 4 participates in sugar binding [7].

The aim of present study was to reinvestigate the topology of rabbit SGLT1 in the region between residues 143–180 using the scanning cysteine accessibility method. We show that by accessibility criteria, multiple residues in this region are located extracellularlly and face an aqueous environment. We also provide functional data confirming a role for residues in TM 4 in the interaction of sugar substrate. Together with the previous structure/function characterization of SGLT1 [6] and molecular dynamic simulation studies [15], our data indicate that the region including residues 162–171 in SGLT1 is a part of transmembrane segment rather than existing as an extracellular connecting loop. This is consistent with the recently reported structure of vSGLT [11].

Materials and methods

Construction of cysteine mutants. The protocols for obtaining the N-terminal myc-tagged cysteine mutations has been described elsewhere [16].

Expression of mutants in COS-7 cells and Western blot detection. COS-7 cells were grown and maintained in RPMI 1640 medium with 10% fetal calf serum and 50 units/ml penicillin/streptomycin (Invitrogen Canada) in a 5% CO_2 at 37 °C. At 70% confluency, the

* Corresponding author. Fax: +1 416 971 2132.
E-mail address: melvin.silverman@utoronto.ca (M. Silverman).

0006-291X/$ - see front matter © 2008 Elsevier Inc. All rights reserved.
doi:10.1016/j.bbrc.2008.11.015

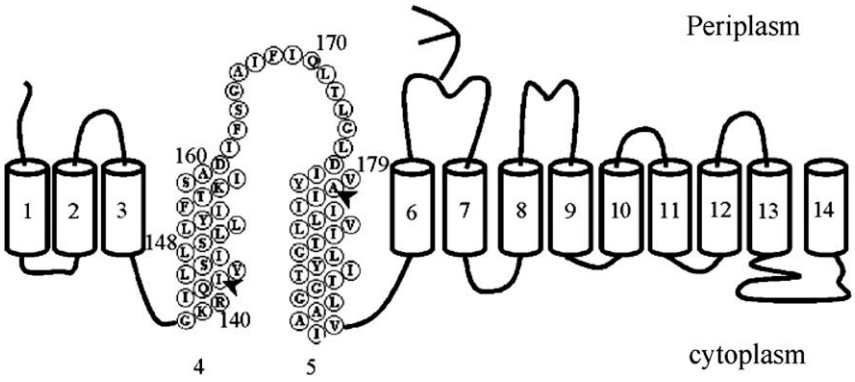

Fig. 1. Model of a modified secondary structure of rabbit SGLT1. The conserved N-glycosylation site is shown by a *Y*. The 38 cysteine-substituted mutants in this study were made from I143 to A180 between TM IV and TM V.

COS-7 cells were transfected with Lipofectamine Plus (Invitrogen) according to manufacturer's protocol.

Proteins samples were resolved on 10% SDS–PAGE and transferred to nitrocellulose. The myc-epitope was detected with mouse monoclonal 9E10 (anti-c-myc, 1:1000) antibody (Berkley Antibody Company), followed by peroxidase conjugated anti-mouse IgG (1:200,000) (Sigma) Immunoblots were developed by chemiluminescence and area analysis was performed using the public domain NIH Image program (National Institutes of Health). Western blot for β-actin was performed to check equal loading.

αMG uptake experiment. [^{14}C] αMG (α-methyl-D-glucopyranoside; Amersham Health, Canada) uptake was prepared as described previously [17]. Culture medium was aspirated, and replaced with 500 μl of incubation medium containing either 140 mM NaCl or 140 mM KCl, 20 mM mannitol, 10 mM HEPES/Tris, pH 7.4 and 1 mM [^{14}C] αMG. After 10 min at room temperature, the incubation medium was aspirated and the wells were washed three times with 3 ml of ice-cold stop buffer, consisting of 140 mM KCl, 20 mM mannitol, 10 mM HEPES/Tris, pH 7.4, and 200 μM phloridzin. The cells were solubilized with 500 ml of PBS buffer with 0.1% SDS. Solubilization proceeded for 20 min, then the solution was removed and prepared for liquid-scintillation counting.

Labeling of surface expressed mutants in COS-7 cells with biotin-MTSEA. Cells in each well (1×0^5 cells/well, 12 well plate) were first preincubated for 10 min at room temperature with either 500 μl PBS (control), 1.35 mM phloridzin or phloretin, and 20 mM αMG, D-glucose or 20 mM L-glucose. The cells in each well were then exposed to 500 μl of 1 mM biotin-MTSEA for 10 min at room temperature. Cells in each well were then washed three times with 2 ml cold PBS and individual wells were scraped into 0.5 ml lysis buffer (50 mM Tris–HCL, 150 mM NaCl, 1% Triton, 1% SDS, 1 mM EDTA and protease inhibitor cocktail). Samples were rocked at 4 °C for 30 min, and the insoluble protein removed by centrifugation at 14,000 rpm for 15 min. Biotin labeled proteins were isolated from the cell lysates with immobilized streptavidin–agarose (Sigma) (10% total volume, about 50 μl) by incubating overnight at 4 °C with gentle agitation. The beads were washed and the biotinylated protein eluted from the beads by the addition of 50 μl SDS–PAGE sample buffer (4% SDS) at 100 °C for 3 min.

Oocyte preparation and injection. Xenopus laevis were prepared as described previously [13]. The injected oocytes were stored at 16–18 °C for 4 days or more.

Electrophysiology and transient current measurements. Voltage clamping and recordings were performed as described previously [12]. The oocytes were constantly superfused with a solution for electrophysiological experiments consisting of 100 mM NaCl, 2 mM KCl, 1 mM $MgCl_2$, 1 mM $CaCl_2$, and 10 mM HEPES–Tris base (pH 7.4) and held at a holding potential (−50 mV), then was subjected to a series of voltage test pulses. *n* is the number of observations.

Pre-steady state currents were determined as described previously [6,18]. The pre-steady state currents for each V_t were integrated over the entire course of the trace to calculate the total charge transferred by the cotransporter. These $Q(V_t)$ curves were fitted to the two-state Boltzmann relation to estimate $V_{0.5}$ (the potential at which half of the total charge transfer is complete), Q_{max} (the total charge transferred) and *z* (the apparent valence of the movable charge).

Steady state parameters were determined with the difference in the steady state currents obtained before and after exposure to the substrate as described previously [6]. The final 100 ms of a test pulse were selected and the average current value of this range was acquired. The average current values were plotted versus [substrate]. These *I* ([S]) curves were fitted to the Hill relation to estimate I_{max} (the maximal current induced at saturating [substrate]) and $K_{0.5}$ (the [S] at which the $I = I_{max}/2$).

Statistical comparisons of means. Data are presented with means ± SEM. Comparisons of parameters were tested with *t*-test (ORIGIN 7, MA). Statistical significance was accepted at an alpha level of $p < 0.05$.

Results

Expression and αMG transport activity of mutants in COS-7 cells

It has been previously demonstrated that N-terminal myc-tagged WT rabbit SGLT1 is expressed at the cell surface of transiently transfected COS-7 cells and its activity is similar to the non-myc-tagged WT rabbit SGLT1 in terms of sugar transport and phloridzin binding [16]. In the present study, we used immunoblotting of myc-tagged mutants in COS-7 cells, chemical modification by MTS derivatives and the two-electrode voltage-clamp method in *X. laevis* oocytes to study the role of residues I143-A180 (Fig. 1).

Table 1 summarizes the Na^+-dependent αMG uptake from COS-7 cells expressing mutants as a percentage of the WT control. The 38 mutants studied retained varying degrees of activity compared with WT. Most mutants exhibited more than 20% of transport activity. Three mutants (Y153, I154C, and G165C) retained only 10–15% activity compared with WT. Another three mutants (K157C, A160C, and D161C) were inactive or had activities less than 5% of the parent transporter despite expression at the cell surface (Fig. 2A), suggesting that these three residues may play functionally important roles in glucose transport in SGLT1.

Table 1
Na^+-dependent αMG uptake of single cysteine-substituted rabbit SGLT1 mutants.

Mutants	% Uptake	Mutants	% Uptake	Mutants	% Uptake	Mutants	% Uptake
I143C	58	Y153C	14	F163C	33	L173C	66
Y144C	86	I154C	9	S164C	26	G174C	32
L145C	100	F155C	64	G165C	12	L175C	74
S146C	92	T156C	50	A166C	49	D176C	100
I147C	96	K157C	2	I167C	64	I177C	75
L148C	91	I158C	27	F168C	31	Y178C	83
S149C	22	S159C	60	I169C	47	V179C	100
L150C	70	A160C	0	Q170C	75	A180C	100
L151C	74	D161C	1	L171C	63		
L152C	77	I162C	26	T172C	69		

COS-7 cells were transfected with empty vector (pMT4), WT or mutants ($n \geqslant 2$). The uptake of αMG was measured as described in the experimental procedures section. The external medium contained 140 mM NaCl, 20 mM mannitol, 10 mM Hepes/Tris, pH 7.4, and 1 mM [^{14}C] αMG. The Na^+-independent uptake of 1 mM [^{14}C] αMG was measured in equivalent medium containing 140 mM KCl. For clarity the Na^+-independent uptake values have been subtracted. Sugar uptakes for the mutants are given as a percentage of that obtained for the wild type rabbit SGLT1.

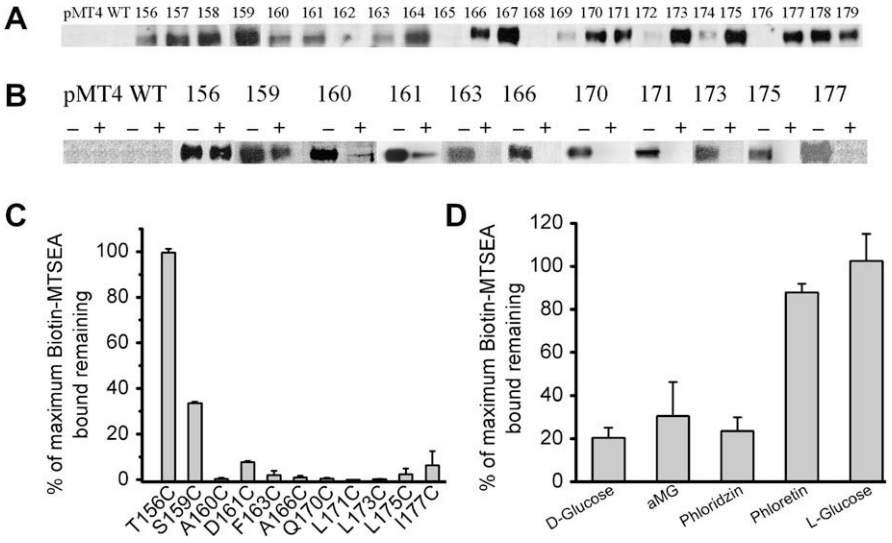

Fig. 2. (A) Biotin-MTSEA reactivity to mutants. (B) MTSES pretreatment protects against biotin-MTSEA reactivity to mutants. COS-7 cells expressing empty vector (pMT4), WT, or mutants, were preincubated in sodium buffer with (+) or without (−) 1 mM MTSES at room temperature for 10 min in order to label the accessible cysteines, washed, and then exposed to biotin-MTSEA at room temperature for 10 min. Cell lysates were collected, reacted with streptavidin-agarose, and bound proteins subjected to immunoblot analysis with anti-myc-antibody. (C) Densitometric tracings for each experiment were analyzed and expressed as a percent of maximum biotin-MTSEA bound (10 min. value). The *error bars* represent SEM ($n \geqslant 3$). (D) Effect of substrate on biotin-MTSEA reactivity to mutant T156C. Densitometric tracings for each experiment were analyzed and expressed as a percent of maximum biotin-MTSEA bound (10 min value). The *error bars* represent SEM ($n \geqslant 3$).

Determination of topology for TMs 4-5

Biotinylation of mutants in intact COS-7 cells

Previous work had demonstrated that biotin-MTSEA does not react with COS-7 cells expressing myc-tagged WT rabbit SGLT1 or empty vector (pMT4) [17]. Therefore, COS-7 cells transfected with vector (pMT4) or WT were used as a negative control in each experiment. The cell surface expression of the 38 mutants (I143C-A180C) in COS-7 cells was measured directly by labeling with biotin-MTSEA. Of the 38 mutants studied, fourteen mutants (I143C-F155C, A180C; Fig. 1) were not labeled by biotin-MTSEA (data not shown). In contrast, twenty mutants between T156C and V179C specifically bound to biotin-MTSEA (Fig. 2A). Finally, five mutants (I162C, G165C, F168C, and D176C) between T156C and V179C were difficult to detect after labeling with MTSEA-biotin due to the low expression and/or steric hindrance.

MTSES accessibility of cysteine mutants expressed in COS-7 cells

We have shown that mutants T156C to V179C could be specifically labeled by biotin-MTSEA (Fig. 2A). Biotin-MTSEA is relatively membrane impermeant [19]. To determine if residues accessible to alkylation by biotin-MTSEA are located in a hydrophilic vs a hydrophobic environment, we tested whether pre-incubation with membrane impermeant MTSES prevents biotin-MTSEA labeling to mutants. Eleven mutants (residues T156 to I177) were chosen for pretreatment with membrane impermeant MTSES. Since WT SGLT1 expressed in COS-7 cells was previously shown to be insensitive to biotin-MTSEA and MTSES [16], COS-7 cells transfected with vector (pMT4) or WT were used as a negative control in each experiment. In Fig. 2B and C, pretreatment of mutants with MTSES showed that (1) nine out of eleven mutants (A160C, D161C, F163C, A166C, Q170C, L171C, L173C, L175C, and I177C) were highly sensitive to MTSES and reactivity with biotin-MTSEA significantly decreased 90%; (2) mutant S159C was also sensitive to MTSES and reactivity with biotin-MTSEA decreased 65%; (3) mutant T156C was not sensitive to MTSES.

Determination of residues' functions in TMs 4-5

Effect of substrate on the accessibility of mutant T156Cin TM IV expressed in COS-7 cells

We were interested in investigating whether this region of rabbit SGLT1 participates in sugar interaction/binding. Accordingly, we studied the apparent competition between sugar substrates

and biotin-MTSEA with respect to biotin-MTSEA reactivity with cysteine mutant-T156C.

Fig. 2D illustrates the results of the relative inhibition of biotin-MTSEA reactivity to mutant T156C in the presence of sugar analogue, SGLT1 specific inhibitor–phloridzin (including the sugar moiety and aglucone part) or phloretin (which lacks the sugar moiety of phloridzin). Inspection of Fig. 2D indicates that mutant T156C was only sensitive to D-glucose, αMG and phloridzin, and decreased biotin-MTSEA binding by 80%, 70%, and 75%, respectively. In contrast, phloretin, and L-glucose had no effect on biotin-MTSEA binding of mutant T156C. These results are consistent with previous studies that demonstrated the order of sugar specificity of WT rabbit SGLT1 to be D-glucose > αMG >> L-glucose [16].

Characterization of cysteine mutants I177C, Y178C, and A180C in TM 5 expressed in Xenopus laevis oocytes

To extend the functional characterization of rabbit SGLT1 in TM 5, we investigated three residues (I177, Y178, and A180), located just below the membrane–water interface at the extracellular end of TM 5. The normal residues were each replaced with cysteine and studied using the two-electrode voltage-clamp method in *Xenopus laevis* oocytes.

Pre-steady state currents for mutants were obtained as a function of voltage and integrated over 300 ms (V_t) to calculate total charge (Q) transferred by the cotransporter (V_h was −50 mV, V_t varied from −150 mV to +70 mV). The charge (Q) was then plotted as a function of the test pulses, and the $Q(V_t)$ curves were fit to the two-state Boltzmann equation. This protocol was carried out at 100 mM saturating Na^+ concentrations and compared to WT rabbit SGLT1. In 100 mM Na^+, the $V_{0.5}$ values of mutants I177C, Y178C and A180C are shifted to negative potentials compared to WT [−28.4 ± 2.3 mV (n = 4), −29.5 ± 2.0 mV (n = 5), −32.4 ± 0.9 mV (n = 3), and −1.5 ± 5.1 mV (n = 5), respectively] (Fig. 3A).

The apparent affinity of mutants for sugar substrate αMG, ($K_{0.5}^{\alpha MG}$), was determined by measuring αMG induced steady state currents at various sugar concentrations and over a range of holding potentials [6]. The results were then fitted according to the Michaelis–Menten equation (Fig. 3B). At −150 mV, the $K_{0.5}^{\alpha MG}$ of mutants I177C, Y178C, and A180C is 0.15 ± 0.01, 0.04 ± 0.01, and 0.08 ± 0.02 mM, respectively; while for WT, $K_{0.5}^{\alpha MG}$ is 0.16 ± 0.01 mM. At −50 mV, the $K_{0.5}^{\alpha MG}$ of mutants I177C, Y178C, and A180C is 0.12 ± 0.02, 0.04 ± 0.01, and 0.10 ± 0.03 mM, respectively; while for WT, $K_{0.5}^{\alpha MG}$ is 0.19 ± 0.02 mM.

To determine the Na^+ affinity of mutants, we measured αMG induced steady state currents (obtained at saturating 5 mM αMG) at various Na^+ concentrations over a range of holding potentials and the resulting curves were analyzed using the Hill relationship (Fig. 3C) [6]. At −150 mV, the $K_{0.5}^{Na+}$ of mutants I177C, Y178C, and A180C is 11.4 ± 1.0, 10.1 ± 0.5, and 14.5 ± 0.1 mM, respectively; while for WT, $K_{0.5}^{\alpha MG}$ is 8.3 ± 0.8 mM. At −50 mV, the $K_{0.5}^{Na+}$ of mutants I177C, Y178C, and A180C is 25.9 ± 0.8, 11.8 ± 0.8, and 34.2 ± 6.8 mM, respectively; while for WT, $K_{0.5}^{\alpha MG}$ is 34.7 ± 1.5 mM.

Discussion

We have used scanning cysteine accessibility methods with thiol-reactive MTS reagents to investigate the topology/functions in the region surrounding predicted TMs 4–5.

MTSES protects mutants (between T156 and V179) from reacting with biotin-MTSEA, suggesting that these residues are on the extracellular side of the membrane or facing an aqueous environment. The results obtained from functional characterization of mutant T156C suggest that TM IV directly or indirectly participates in sugar binding because sugar substrates (D-glucose, αMG and phloridzin), but not phloretin and L-glucose protect mutant T156C from reactivity to biotin-MTSEA (Fig. 2D). Further, since mutants I177C, Y178C, and A180C exhibited altered voltage sensitivity and increased Na^+ and sugar affinity of the cotransporter, this suggests that while this region of TM V is not di-

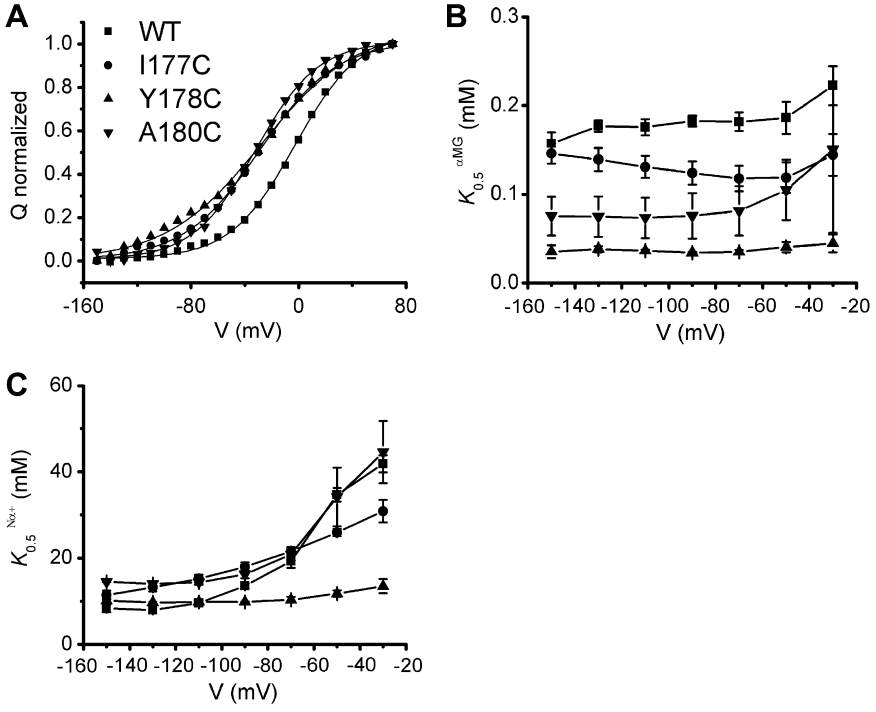

Fig. 3. (A) Typical results demonstrating the effects on WT or mutants charge transfer in oocytes in 100 mM Na^+. The $Q(V_t)$ curves were adjusted to zero at hyperpolarizing voltages (−150 mV) and normalized with respect to the extrapolated Q_{max}. (B) The αMG $K_{0.5}$ of WT (n = 5) and mutants ($n \geqslant 3$) for voltage dependence. The *error bars* represent SEM. (C) The Na^+ $K_{0.5}$ of WT (n = 4) and mutants (n = 3) for voltage dependence. The *error bars* represent SEM.

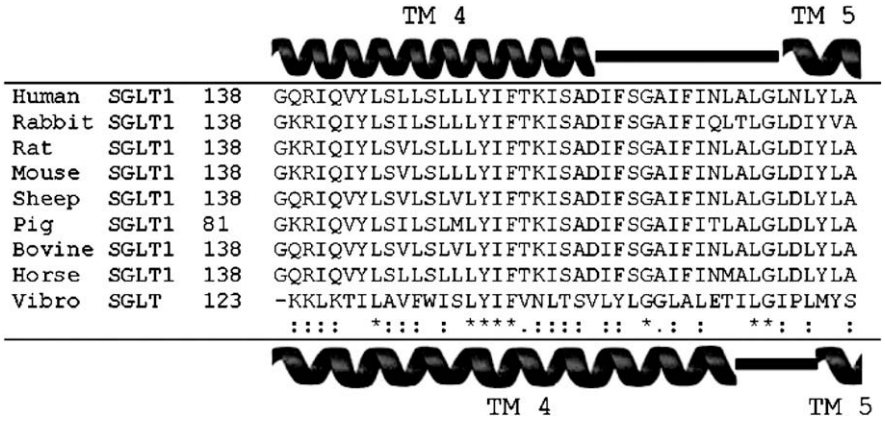

Fig. 4. Amino acid sequence alignment and secondary structure of the transmembrane segments 4–5 in SGLT1 and vSGLT. The previously predicted topology of SGLT1 is shown on top. The secondary structure of vSGLT is shown on bottom.

rectly involved in binding of sugar substrate, residues at this location are likely involved in determining accessibility to the Na^+-and sugar-binding domain.

The 3D structure of vSGLT, a homolog of SGLT1, was recently determined and provides important insights into the structure/function of this bacterial cotransporter [11]. Although there are significant functional differences between vSGLT and mammalian SGLT1 (the Na^+/galactose stoichiometry is 1:1 and the Na^+/glucose stoichiometry is 2:1, respectively), it is informative to explore how much of the information obtained from vSGLT structure can be extrapolated to SGLT1. The crystal structure of vSGLT contains a hydrophilic core structure formed by multiple transmembrane helices from both N-terminus (TMs 2–6) and C-terminus (TMs 7–11). Na^+ and galactose are bound in the center of the core. The theme of N- and C-terminal segments participating in formation of a common cavity for Na^+ and cotransported substrate is also emerging from studies of other ion coupled cotransporters, such as the Na^+/leucine transporter [20], Na^+/aspartate transporter [21], Na^+/glutamate transporter [22], Na^+/H^+ antiporter [23] and lactose permease [24]). For example, crystal studies of lactose permease complexed with lactose demonstrate the involvement of TM I, IV, and V in sugar binding [24].

In the region (143–180), vSGLT has a sequence similarity of 76% to all members of SGLT1 (Fig. 4). Therefore, it is possible that the topologies in this region surrounding predicted TMs 4–5 of vSGLT and SGLT1 are similar. Previous cysteine scanning mutagenesis (amino acids 162–173 of rabbit SGLT1) in *Xenopus laevis* oocytes indicated that this region might be α-helix with one face exposed to the extracellular aqueous environment [6]. Molecular dynamics (MD) simulations at low dielectric constant that were carried out for a 42-residue peptide (amino acids 147–188 of human SGLT1) also were consistent with the conclusion that the segment 162–173 has an α-helical conformation [15]. Taken together, the present study along with previous biochemical characterization of SGLT1 [6,7,12–14], shows that segment 143–171 is part of TM 4 and that TMs 4–5 in the N-terminal half of SGLT1 form part of aqueous Na^+- and sugar-binding cavity. Collectively, our results support the conclusion that the published crystal structure of vSGLT can be extended to mammalian SGLT1.

Acknowledgment

This work was supported by Canadian Institutes of Health Research Grant MOP-15267.

References

[1] M.G. Martin, E. Turk, M.P. Lostao, C. Kerner, E.M. Wright, Defects in Na+/glucose cotransporter (SGLT1) trafficking and function cause glucose–galactose malabsorption, Nat. Genet. 12 (1996) 216–220.
[2] D. Balen, M. Ljubojevic, D. Breljak, H. Brzica, V. Zlender, H. Koepsell, I. Sabolic, Revised immunolocalization of the Na^+ D-glucose cotransporter SGLT1 in rat organs with an improved antibody, Am. J. Physiol. Cell Physiol. 295 (2008) C475–C489.
[3] A.J. Hirsh, C.I. Cheeseman, Cholecystokinin decreases intestinal hexose absorption by a parallel reduction in SGLT1 abundance in the brush-border membrane, J. Biol. Chem. 273 (1998) 14545–14549.
[4] Y. Ikumi, T. Kida, S. Sakuma, S. Yamashita, M. Akashi, Polymer-phloridzin conjugates as an anti-diabetic drug that inhibits glucose absorption through the Na+/glucose cotransporter (SGLT1) in the small intestine, J. Control Release 125 (2008) 42–49.
[5] E. Turk, E.M. Wright, Membrane topology motifs in the SGLT cotransporter family, J. Membr. Biol. 159 (1997) 1–20.
[6] B. Lo, M. Silverman, Cysteine scanning mutagenesis of the segment between putative transmembrane helices IV and V of the high affinity Na+/Glucose cotransporter SGLT1. Evidence that this region participates in the Na+ and voltage dependence of the transporter, J. Biol. Chem. 273 (1998) 29341–29351.
[7] T. Liu, B. Lo, P. Speight, M. Silverman, Transmembrane IV of the high-affinity sodium-glucose cotransporter participates in sugar binding, Am. J. Physiol. Cell Physiol. 295 (2008) C64–C72.
[8] B.A. Hirayama, D.D. Loo, A. Diez-Sampedro, D.W. Leung, A.K. Meinild, M. Lai-Bing, E. Turk, E.M. Wright, Sodium-dependent reorganization of the sugar-binding site of SGLT1, Biochemistry 46 (2007) 13391–13406.
[9] D.G. Gagnon, P. Bissonnette, J.Y. Lapointe, Identification of a disulfide bridge linking the fourth and the seventh extracellular loops of the na+/glucose cotransporter, J. Gen. Physiol. 127 (2006) 145–158.
[10] T. Puntheeranurak, M. Kasch, X. Xia, P. Hinterdorfer, R.K. Kinne, Three surface subdomains form the vestibule of the Na+/glucose cotransporter SGLT1, J. Biol. Chem. 282 (2007) 25222–25230.
[11] S. Faham, A. Watanabe, G.M. Besserer, D. Cascio, A. Specht, B.A. Hirayama, E.M. Wright, J. Abramson, The crystal structure of a sodium galactose transporter reveals mechanistic insights into Na^+/sugar symport, Science 321 (2008) 810–814.
[12] B. Lo, M. Silverman, Replacement of Ala-166 with cysteine in the high affinity rabbit sodium/glucose transporter alters transport kinetics and allows methanethiosulfonate ethylamine to inhibit transporter function, J. Biol. Chem. 273 (1998) 903–909.
[13] S.A. Huntley, D. Krofchick, M. Silverman, Position 170 of rabbit Na+/glucose cotransporter (rSGLT1) Lies in the Na+ pathway; modulation of polarity/charge at this site regulates charge transfer and carrier turnover, Biophys. J. 87 (2004) 295–310.
[14] S.A. Huntley, D. Krofchick, M. Silverman, A glutamine to glutamate mutation at position 170 (Q170E) in the rabbit Na+/glucose cotransporter, rSGLT1, enhances binding affinity for Na+, Biochemistry 45 (2006) 4653–4663.
[15] V. Khutorsky, Alpha-hairpin stability and folding of transmembrane segments, Biochem. Biophys. Res. Commun. 301 (2003) 31–34.
[16] S. Vayro, B. Lo, M. Silverman, Functional studies of the rabbit intestinal Na^+/glucose carrier (SGLT1) expressed in COS-7 cells: evaluation of the mutant A166C indicates this region is important for Na^+ activation of the carrier, Biochem. J. 332 (1998) 119–125.
[17] S. Vayro, M. Silverman, PKC regulates turnover rate of rabbit intestinal Na+ glucose transporter expressed in COS-7 cells, Am. J. Physiol. 276 (1999) C1053–C1060.
[18] D. Krofchick, M. Silverman, Investigating the conformational states of the rabbit Na(+)/glucose cotransporter, Biophys. J. 84 (2003) 3690–3702.

[19] J.A. Teissere, C. Czajkowski, A (beta)-strand in the (gamma)2 subunit lines the benzodiazepine binding site of the GABA A receptor: structural rearrangements detected during channel gating, J. Neurosci. 21 (2001) 4977–4986.
[20] A. Yamashita, S.K. Singh, T. Kawate, Y. Jin, E. Gouaux, Crystal structure of a bacterial homologue of Na^+/Cl^--dependent neurotransmitter transporters, Nature 437 (2005) 215–223. Epub 2005 July 24.
[21] O. Boudker, R.M. Ryan, D. Yernool, K. Shimamoto, E. Gouaux, Coupling substrate and ion binding to extracellular gate of a sodium-dependent aspartate transporter, Nature 445 (2007) 387–393. Epub 2007 January 17.
[22] D. Yernool, O. Boudker, Y. Jin, E. Gouaux, Structure of a glutamate transporter homologue from *Pyrococcus horikoshii*, Nature 431 (2004) 811–818.
[23] C. Hunte, E. Screpanti, M. Venturi, A. Rimon, E. Padan, H. Michel, Structure of a Na^+/H^+ antiporter and insights into mechanism of action and regulation by pH, Nature 435 (2005) 1197–1202.
[24] J. Abramson, I. Smirnova, V. Kasho, G. Verner, H.R. Kaback, S. Iwata, Structure and mechanism of the lactose permease of *Escherichia coli*, Science 301 (2003) 610–615.